Available online at www.sciencedirect.com

SciVerse ScienceDirect

Nuclear Physics B 867 (2013) 1–18

NUCLEAR PHYSICS B

www.elsevier.com/locate/nuclphysb

Measurement of the ratio of branching fractions $\mathcal{B}(B^0 \to K^{*0}\gamma)/\mathcal{B}(B_s^0 \to \phi\gamma)$ and the direct CP asymmetry in $B^0 \to K^{*0}\gamma$ ☆

LHCb Collaboration

Received 4 September 2012; accepted 20 September 2012

Available online 24 September 2012

Abstract

The ratio of branching fractions of the radiative B decays $B^0 \to K^{*0}\gamma$ and $B_s^0 \to \phi\gamma$ has been measured using an integrated luminosity of 1.0 fb^{-1} of pp collision data collected by the LHCb experiment at a centre-of-mass energy of $\sqrt{s} = 7$ TeV. The value obtained is

$$\frac{\mathcal{B}(B^0 \to K^{*0}\gamma)}{\mathcal{B}(B_s^0 \to \phi\gamma)} = 1.23 \pm 0.06\ (\text{stat.}) \pm 0.04\ (\text{syst.}) \pm 0.10\ (f_s/f_d),$$

where the first uncertainty is statistical, the second is the experimental systematic uncertainty and the third is associated with the ratio of fragmentation fractions f_s/f_d. Using the world average value for $\mathcal{B}(B^0 \to K^{*0}\gamma)$, the branching fraction $\mathcal{B}(B_s^0 \to \phi\gamma)$ is measured to be $(3.5 \pm 0.4) \times 10^{-5}$.

The direct CP asymmetry in $B^0 \to K^{*0}\gamma$ decays has also been measured with the same data and found to be

$$\mathcal{A}_{CP}\big(B^0 \to K^{*0}\gamma\big) = \big(0.8 \pm 1.7\ (\text{stat.}) \pm 0.9\ (\text{syst.})\big)\%.$$

Both measurements are the most precise to date and are in agreement with the previous experimental results and theoretical expectations.

☆ © CERN for the benefit of the LHCb Collaboration.

issn/
http://dx.doi.org/10.1016/j.nuclphysb.2012.09.013

1. Introduction

In the Standard Model (SM), the decays[1] $B^0 \to K^{*0}\gamma$ and $B_s^0 \to \phi\gamma$ proceed at leading order through the electromagnetic penguin transitions, $b \to s\gamma$. At one-loop level these transitions are dominated by a virtual intermediate top quark coupling to a W boson. Extensions of the SM predict additional one-loop contributions that can introduce sizeable changes to the dynamics of the transition [1].

Radiative decays of the B^0 meson were first observed by the CLEO Collaboration in 1993 in the decay mode $B^0 \to K^{*0}\gamma$ [2]. In 2007 the Belle Collaboration reported the first observation of the analogous decay in the B_s^0 sector, $B_s^0 \to \phi\gamma$ [3]. The current world averages of the branching fractions of $B^0 \to K^{*0}\gamma$ and $B_s^0 \to \phi\gamma$ are $(4.33 \pm 0.15) \times 10^{-5}$ and $(5.7^{+2.1}_{-1.8}) \times 10^{-5}$, respectively [4,5]. These results are in agreement with the latest theoretical predictions from NNLO calculations using soft-collinear effective theory [6], $\mathcal{B}(B^0 \to K^{*0}\gamma) = (4.3 \pm 1.4) \times 10^{-5}$ and $\mathcal{B}(B_s^0 \to \phi\gamma) = (4.3 \pm 1.4) \times 10^{-5}$, which suffer from large uncertainties from hadronic form factors. A better-predicted quantity is the ratio of branching fractions, as it benefits from partial cancellations of theoretical uncertainties. The two branching fraction measurements lead to a ratio $\mathcal{B}(B^0 \to K^{*0}\gamma)/\mathcal{B}(B_s^0 \to \phi\gamma) = 0.7 \pm 0.3$, while the SM prediction is 1.0 ± 0.2 [6]. When comparing the experimental and theoretical branching fraction for the $B_s^0 \to \phi\gamma$ decay, it is necessary to account for the large decay width difference in the B_s^0–$\bar{B}_s^0$ system. This can give rise to a correction on the theoretical branching fraction as large as 9% as described in [7].

The direct CP asymmetry in the $B^0 \to K^{*0}\gamma$ decay is defined as $\mathcal{A}_{CP} = [\Gamma(\bar{B}^0 \to \bar{f}) - \Gamma(B^0 \to f)]/[\Gamma(\bar{B}^0 \to \bar{f}) + \Gamma(B^0 \to f)]$. The SM prediction, $\mathcal{A}_{CP}^{\rm SM}(B^0 \to K^{*0}\gamma) = (-0.61 \pm 0.43)\%$ [8], is affected by a smaller theoretical uncertainty from the hadronic form factors than the branching fraction calculation. The precision on the current experimental value, $\mathcal{A}_{CP}(B^0 \to K^{*0}\gamma) = (-1.6 \pm 2.2 \pm 0.7)\%$ [5,9], is statistically limited and more precise measurements would constrain contributions from beyond the SM scenarios, some of which predict that this asymmetry could be as large as -15% [10].

This paper presents a measurement of $\mathcal{B}(B^0 \to K^{*0}\gamma)/\mathcal{B}(B_s^0 \to \phi\gamma)$ using 1.0 fb^{-1} of data taken with the LHCb detector. The measured ratio and the world average value of $\mathcal{B}(B^0 \to K^{*0}\gamma)$ are then used to determine $\mathcal{B}(B_s^0 \to \phi\gamma)$. This result supersedes a previous LHCb measurement based on an integrated luminosity of 0.37 fb^{-1} of data at $\sqrt{s} = 7$ TeV [11]. A measurement of the direct CP asymmetry of the decay $B^0 \to K^{*0}\gamma$ is also presented.

2. The LHCb detector and dataset

The LHCb detector [12] is a single-arm forward spectrometer covering the pseudorapidity range $2 < \eta < 5$, designed for the study of particles containing b or c quarks. The detector includes a high precision tracking system consisting of a silicon-strip vertex detector surrounding the pp interaction region, a large-area silicon-strip detector located upstream of a dipole magnet with a bending power of about 4 Tm, and three stations of silicon-strip detectors and straw drift tubes placed downstream. The combined tracking system has a momentum resolution $\Delta p/p$ that varies from 0.4% at 5 GeV/c to 0.6% at 100 GeV/c, and an impact parameter (IP) resolution of 20 μm for tracks with high transverse momentum ($p_{\rm T}$). Charged hadrons are identified using two ring-imaging Cherenkov detectors (RICH). Photon, electron and hadron candidates are

[1] Unless stated otherwise, charge conjugated modes are implicitly included throughout this paper.

identified by a calorimeter system consisting of scintillating-pad and preshower detectors, an electromagnetic calorimeter and a hadronic calorimeter. Muons are identified by a system composed of alternating layers of iron and multiwire proportional chambers. The trigger consists of a hardware stage, based on information from the calorimeter and muon systems, followed by a software stage which applies a full event reconstruction.

Decay candidates are required to have triggered on the signal photon and the daughters of the vector meson. At the hardware stage, the decay candidates must have been triggered by an electromagnetic candidate with transverse energy ($E_{\rm T}$) > 2.5 GeV. The software stage is divided into two steps. The first one performs a partial event reconstruction and reduces the rate such that the second can perform full event reconstruction to further reduce the data rate. At the first software stage, events are selected when a charged track is reconstructed with IP $\chi^2 > 16$. The IP χ^2 is defined as the difference between the χ^2 of the pp interaction vertex (PV) fit reconstructed with and without the considered track. Furthermore, a charged track is required to have either $p_{\rm T} > 1.7\,{\rm GeV}/c$ for a photon with $E_{\rm T} > 2.5$ GeV or $p_{\rm T} > 1.2\,{\rm GeV}/c$ when the photon has $E_{\rm T} > 4.2$ GeV. At the second software stage, a track passing the previous criteria must form a K^{*0} or ϕ candidate when combined with an additional track, and the invariant mass of the combination of the $K^{*0}(\phi)$ candidate and the photon candidate that triggered the hardware stage is required to be within 1 GeV/c^2 of the world average B^0 (B_s^0) mass. The data used for this analysis correspond to 1.0 fb^{-1} of pp collisions collected in 2011 at the LHC with a centre-of-mass energy of $\sqrt{s} = 7$ TeV.

Large samples of $B^0 \to K^{*0}\gamma$ and $B_s^0 \to \phi\gamma$ Monte Carlo simulated events are used to optimise the signal selection and to parametrise the invariant-mass distribution of the B meson. Possible contamination from specific background channels has also been studied using dedicated simulated samples. For the simulation, pp collisions are generated using PYTHIA 6.4 [13] with a specific LHCb configuration [14]. Decays of hadronic particles are described by EVTGEN [15] in which final state radiation is generated using PHOTOS [16]. The interaction of the generated particles with the detector and its response are implemented using the GEANT4 toolkit [17] as described in Ref. [18].

3. Offline event selection

The selection of $B^0 \to K^{*0}\gamma$ and $B_s^0 \to \phi\gamma$ decays is designed to maximise the cancellation of uncertainties in the ratio of their selection efficiencies.

The charged tracks used to build the vector mesons are required to have $p_{\rm T} > 500\,{\rm MeV}/c$, with at least one of them having $p_{\rm T} > 1.2\,{\rm GeV}/c$. In addition, a requirement of IP $\chi^2 > 25$ means that they must be incompatible with coming from any PV. The charged tracks are identified as either kaons or pions using information provided by the RICH system. This is based on the comparison between the two particle hypotheses. Kaons (pions) in the studied $B \to V\gamma$ decays, where V stands for the vector meson, are identified with a $\sim 70(83)\%$ efficiency for a $\sim 3(2)\%$ pion (kaon) contamination.

Photon candidates are required to have $E_{\rm T} > 2.6$ GeV. Neutral and charged clusters in the electromagnetic calorimeter are separated based on their compatibility with extrapolated tracks [19] while photon deposits are distinguished from π^0 deposits using the shape of the showers in the electromagnetic calorimeter.

Oppositely-charged kaon–pion (kaon–kaon) combinations are accepted as K^{*0} (ϕ) candidates if they form a good quality vertex and have an invariant mass within ± 50 (± 10) MeV/c^2 of the world average K^{*0} (ϕ) mass [9]. The resulting vector meson candidate is combined with

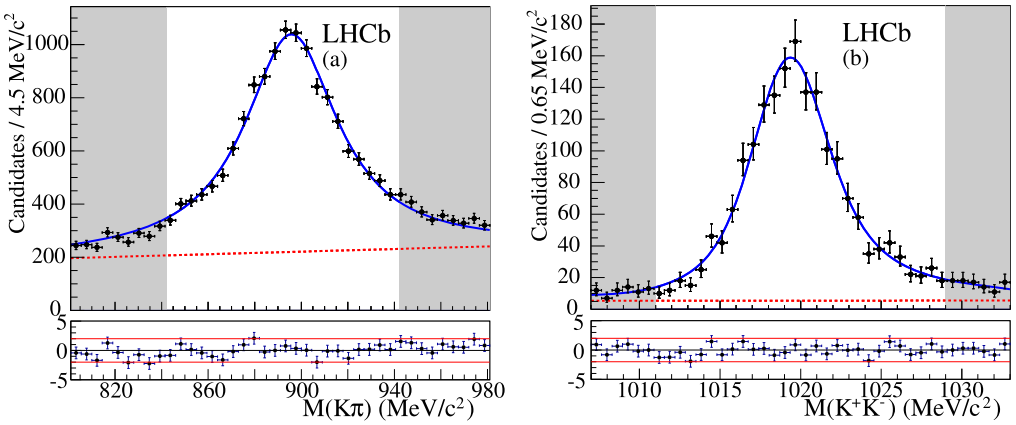

Fig. 1. Invariant-mass distributions of the (a) K^{*0} and (b) ϕ resonance candidates. The black points represent the data and the fit result is represented as a solid blue line. The fit is described in the text. The regions outside the vector meson invariant-mass window are shaded. The Poisson χ^2 residuals [22] are shown below the fits with the $\pm 2\sigma$ confidence-level interval delimited by solid red lines. (For interpretation of the references to colours in this figure, the reader is referred to the web version of this article.)

the photon candidate to make a B candidate. The invariant-mass resolution of the selected B candidate is ≈ 100 MeV$/c^2$ for the decays presented in this paper.

The B candidates are required to have an invariant mass within 1 GeV$/c^2$ of the world average B mass [9] and to have $p_{\mathrm{T}} > 3$ GeV$/c$. They must also point to a PV, with IP $\chi^2 < 9$, and the angle between the B candidate momentum direction and the B line of flight has to be less than 20 mrad. In addition, the vertex separation χ^2 between the B meson vertex and its related PV must be larger than 100. The distribution of the helicity angle θ_{H}, defined as the angle between the momentum of any of the daughters of the vector meson and the momentum of the B candidate in the rest frame of the vector meson, is expected to follow a $\sin^2\theta_{\mathrm{H}}$ function for $B \to V\gamma$, and a $\cos^2\theta_{\mathrm{H}}$ function for the $B \to V\pi^0$ background. A requirement of $|\cos\theta_{\mathrm{H}}| < 0.8$ is therefore made to reduce $B \to V\pi^0$ background, where the neutral pion is misidentified as a photon. Background coming from partially reconstructed B-hadron decays is reduced by requiring the B vertex to be isolated: its χ^2 must increase by more than two units when adding any other track in the event.

4. Signal and background description

The signal yields of the $B^0 \to K^{*0}\gamma$ and $B_s^0 \to \phi\gamma$ decays are determined from an extended unbinned maximum-likelihood fit performed simultaneously to the invariant-mass distributions of the B^0 and B_s^0 candidates. A constraint on the B^0 and B_s^0 masses is included in the fit which requires the difference between them to be consistent with the LHCb measurement of 87.3 ± 0.4 MeV$/c^2$ [20]. The K^{*0} and ϕ resonances are described by a relativistic P-wave Breit–Wigner distribution [21] convoluted with a Gaussian distribution to take into account the detector resolution. The natural width of the resonances is fixed to the world average value [9]. A polynomial line shape is added to describe the background. The resulting distribution is fitted to the vector meson invariant-mass distribution, as shown in Fig. 1.

The fit to the invariant mass of the vector meson candidates yields a resonance mass of 895.7 ± 0.4 MeV and 1019.42 ± 0.09 MeV for the K^{*0} and ϕ, respectively, in agreement with the world

average values [9]. The detector resolution extracted from the fit is 5 ± 4 MeV for the K^{*0} resonance and 1.3 ± 0.1 MeV for the ϕ. The effect of taking the value found in data or the world average as the central value of the vector meson mass window is negligible. In addition no systematic uncertainty due to the choice of the line shape of the resonances is assigned.

Both $B^0 \to K^{*0}\gamma$ and $B_s^0 \to \phi\gamma$ signal distributions are parametrised with a two-sided Crystal Ball distribution [23]. In the low-mass region, there can be possible losses in the photon energy due to the fiducial volume of the calorimeter. A tail at high masses is also observed and can be explained by the spread in the error of the reconstructed B mass and pile-up effects in the photon deposition. The parameters describing the tails on both sides are fixed to the values determined from simulation. The width of each signal peak is left as a free parameter in the fit.

The reconstructed mass distribution of the combinatorial background has been determined from the low-mass sideband of the K^{*0} mass distribution as an exponential function with different attenuation constants for the two decay channels. Additional contamination from several exclusive background decays is studied using simulated samples. The irreducible $B_s^0 \to K^*\gamma$ decays, the $\Lambda_b^0 \to \Lambda^*(pK^-)\gamma$ decays,[2] and the charmless $B_{(s)}^0 \to h^+h'^-\pi^0$ decays produce peaked contributions under the invariant-mass peak of $B^0 \to K^{*0}\gamma$. As the experimental branching fractions of the charmless B_s^0 and Λ_b^0 decays are unknown, the corresponding contamination rates are estimated either using the predicted branching fraction in the case of $B_s^0 \to K^{*0}\gamma$ decays, assuming SU(3) symmetry for $B_s^0 \to h^+h'^-\pi^0$ decays, or by directly estimating the signal yield from an independent sample as in $\Lambda_b^0 \to \Lambda^*\gamma$ decays. The overall contribution from these decays is estimated to represent $(2.6 \pm 0.4)\%$ and $(0.9 \pm 0.6)\%$ of the $B^0 \to K^{*0}\gamma$ and $B_s^0 \to \phi\gamma$ yields, respectively. Each of these contributions is modelled with a Crystal Ball function determined from a simulated sample and their yields are fixed in the fit.

The partial reconstruction of the charged $B \to h^+h'^-\gamma X$ or $B \to h^+h'^-\pi^0 X$ decays gives a broad contribution at lower candidate masses, with a high-mass tail that extends into the signal region. The partially reconstructed $B^+ \to K^{*0}\pi^+\gamma$ and $B^+ \to \phi K^+\gamma$ radiative decays produce a peaking contribution in the low-mass sideband at around 5.0 GeV/c^2 for $B^0 \to K^{*0}\gamma$ and around 4.5 GeV/c^2 for $B_s^0 \to \phi\gamma$. The corresponding contamination has been estimated to be $(3.3 \pm 1.1)\%$ and $(1.8 \pm 0.3)\%$ for the $B^0 \to K^{*0}\gamma$ and $B_s^0 \to \phi\gamma$ decays, respectively. The partially reconstructed neutral B meson decays also contribute at the same level and several other channels exhibit a similar final state topology. These contributions are described by a Crystal Ball function and the yields are left to vary in the fit. The parameters of the Crystal Ball function are determined from the simulation. Additional contributions from the partial reconstruction of multi-body charmed decays and $B \to V\pi^0\mathrm{X}$ have been added to the simultaneous fit in the same way. The shape of these contributions, again determined from the simulation, follows an ARGUS function [24] peaking around 4.0 GeV/c^2. The various background contributions included in the fit model are summarised in Table 1.

At the trigger level, the electromagnetic calorimeter calibration is different from that in the offline analysis. Therefore, the ± 1 GeV/c^2 mass-window requirement imposed by the trigger causes a bias in the B meson acceptance to appear near the limits of this window. The inefficiency at the edges of the mass window is modelled by including a three-parameter threshold function in the fit model

$$T(m_B) = \left(1 - \mathrm{erf}\left(\frac{m_B - t_\mathrm{L}}{\sqrt{2}\sigma_\mathrm{d}}\right)\right) \times \left(1 - \mathrm{erf}\left(\frac{t_\mathrm{U} - m_B}{\sqrt{2}\sigma_\mathrm{d}}\right)\right), \tag{1}$$

[2] Λ^* stands for $\Lambda(1520)$ and other b-baryon resonances promptly decaying into a pK^- final state.

Table 1
Expected contributions to the $B^0 \to K^{*0}\gamma$ and $B_s^0 \to \phi\gamma$ yields in the ± 1 GeV/c^2 mass window from the exclusive background channels: radiative decays, $h^+h'^-\gamma$ (top), charmless b decays involving energetic π^0, $h^+h'^-\pi^0$ (middle) and partially reconstructed decays (bottom). The average measurement (exp.) or theoretical (theo.) branching fraction is given where available. Each exclusive contribution above 0.1% is included in the fit model, with a fixed shape determined from simulation. The amplitude of the partially reconstructed backgrounds is left to vary in the fit while the $h^+h'^-\gamma$ and $h^+h'^-\pi^0$ contributions are fixed to their expected level.

Decay	Branching fraction ($\times 10^6$)	Relative contribution to $B^0 \to K^{*0}\gamma$	$B_s^0 \to \phi\gamma$
$\Lambda_b^0 \to \Lambda^*\gamma$	estimated from data	$(1.0 \pm 0.3)\%$	$(0.4 \pm 0.3)\%$
$B_s^0 \to K^{*0}\gamma$	1.26 ± 0.31 (theo. [25])	$(0.8 \pm 0.2)\%$	$\mathcal{O}(10^{-4})$
$B^0 \to K^+\pi^-\pi^0$	$35.9^{+2.8}_{-2.4}$ (exp. [4])	$(0.5 \pm 0.1)\%$	$\mathcal{O}(10^{-4})$
$B_s^0 \to K^+\pi^-\pi^0$	estimated from SU(3) symmetry	$(0.2 \pm 0.2)\%$	$\mathcal{O}(10^{-4})$
$B_s^0 \to K^+K^-\pi^0$	estimated from SU(3) symmetry	$\mathcal{O}(10^{-4})$	$(0.5 \pm 0.5)\%$
$B^+ \to K^{*0}\pi^+\gamma$	20^{+7}_{-6} (exp. [4])	$(3.3 \pm 1.1)\%$	$< 6 \times 10^{-4}$
$B^0 \to K^+\pi^-\pi^0\gamma$	41 ± 4 (exp. [4])	$(4.5 \pm 1.7)\%$	$\mathcal{O}(10^{-4})$
$B^+ \to \phi K^+\gamma$	3.5 ± 0.6 (exp. [4])	3×10^{-4}	$(1.8 \pm 0.3)\%$
$B \to V\pi^0 X$	$\mathcal{O}(10\%)$ (exp. [4])	a few%	a few%

where erf is the Gauss error function. The parameter t_L (t_U) represents the actual lower (upper) mass threshold and σ_d is the resolution.

5. Measurement of the ratio of branching fractions

The ratio of branching fractions is measured as

$$\frac{\mathcal{B}(B^0 \to K^{*0}\gamma)}{\mathcal{B}(B_s^0 \to \phi\gamma)} = \frac{N_{B^0 \to K^{*0}\gamma}}{N_{B_s^0 \to \phi\gamma}} \times \frac{\mathcal{B}(\phi \to K^+K^-)}{\mathcal{B}(K^{*0} \to K^+\pi^-)} \times \frac{f_s}{f_d} \times \frac{\epsilon_{B_s^0 \to \phi\gamma}}{\epsilon_{B^0 \to K^{*0}\gamma}}, \tag{2}$$

where N are the observed yields of signal candidates, $\mathcal{B}(\phi \to K^+K^-)/\mathcal{B}(K^{*0} \to K^+\pi^-) = 0.735 \pm 0.008$ [9] is the ratio of branching fractions of the vector mesons, $f_s/f_d = 0.267^{+0.021}_{-0.020}$ [26] is the ratio of the B^0 and B_s^0 hadronization fractions in pp collisions at $\sqrt{s} = 7$ TeV and $\epsilon_{B_s^0 \to \phi\gamma}/\epsilon_{B^0 \to K^{*0}\gamma}$ is the ratio of total reconstruction and selection efficiencies of the two decays.

The results of the fit are shown in Fig. 2. The number of $B^0 \to K^{*0}\gamma$ and $B_s^0 \to \phi\gamma$ candidates is 5279 ± 93 and 691 ± 36, respectively, corresponding to a yield ratio of 7.63 ± 0.38. The relative contamination from partially reconstructed radiative decays is fitted to be $(15 \pm 5)\%$ for $B^0 \to K^{*0}\gamma$ and $(5 \pm 3)\%$ for $B_s^0 \to \phi\gamma$, in agreement with the expected rate from $B^{+(0)} \to K^{*0}\pi^{+(0)}\gamma$ and $B^{+(0)} \to \phi K^{+(0)}\gamma$, respectively. The contribution from partial reconstruction of charmed decays at low mass is fitted to be $(5 \pm 4)\%$ and $(0^{+9}_{-0})\%$ of the $B^0 \to K^{*0}\gamma$ and $B_s^0 \to \phi\gamma$ yields, respectively.

The systematic uncertainty from the background modelling is determined by varying the parameters that have been kept constant in the fit of the invariant-mass distribution within their uncertainty. The 95% CL interval of the relative variation on the yield ratio is determined to be $[-1.2, +1.4]\%$ and is taken as a conservative estimate of the systematic uncertainty associated with the background modelling. The relative variation is dominated by the effect from the partially reconstructed background. This procedure is repeated to evaluate the systematic uncertainty from the signal-shape modelling, by varying the parameters of the Crystal Ball tails within

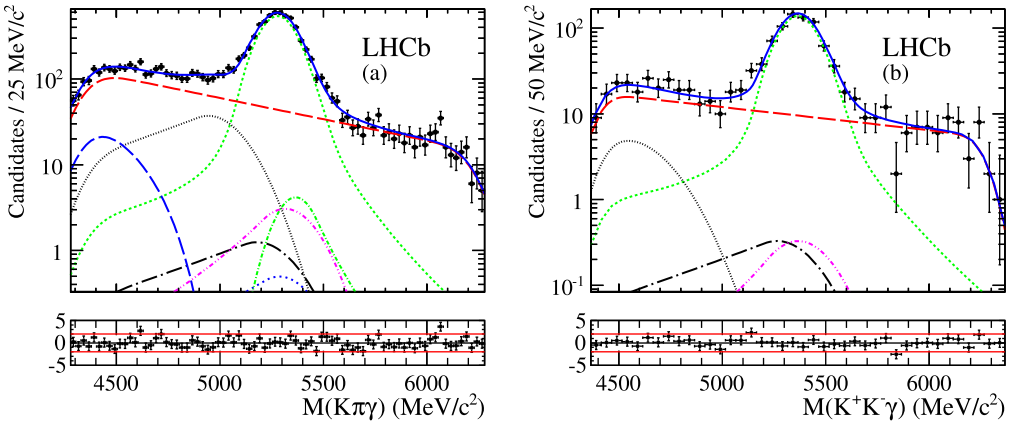

Fig. 2. Invariant-mass distributions of the (a) $B^0 \to K^{*0}\gamma$ and (b) $B_s^0 \to \phi\gamma$ candidates. The black points represent the data and the fit result is represented as a solid blue line. The signal is fitted with a double-sided Crystal Ball function (short-dashed green line). The combinatorial background is modelled with an exponential function (long-dashed red line). In decreasing amplitude order, the exclusive background contributions to $B^0 \to K^{*0}\gamma$ are $B^{+(0)} \to K^{*0}\pi^{+(0)}\gamma$ (short-dotted black), $B \to K^{*0}(\phi)\pi^0 X$ (long-dashed blue), $B_s^0 \to K^{*0}\gamma$ (dotted short-dashed green), $\Lambda_b^0 \to \Lambda^*\gamma$ (double-dotted dashed pink), $B^0 \to K^+\pi^-\pi^0$ (dotted long-dashed black) and $B_s^0 \to K^+\pi^-\pi^0$ (long-dotted blue). The background contributions to $B_s^0 \to \phi\gamma$ are $B^{+(0)} \to \phi K^{+(0)}\gamma$ (dotted black), $\Lambda_b^0 \to \Lambda^*\gamma$ (double-dotted dashed pink) and $B_s^0 \to K^+K^-\pi^0$ (dotted–dashed black). No significant contribution to $B_s^0 \to \phi\gamma$ is found from partially reconstructed $B \to K^{*0}(\phi)\pi^0 X$ decays. The Poisson χ^2 residuals [22] are shown below the fit with the $\pm 2\sigma$ confidence-level interval delimited by solid red lines. (For interpretation of the references to colours in this figure, the reader is referred to the web version of this article.)

their uncertainty. A relative variation of $[-1.3, +1.4]\%$ on the yield ratio is observed and added to the systematic uncertainty. As a cross-check of the possible bias introduced on the ratio by the modelling of the mass-window thresholds and the partially reconstructed background that populates the low-mass region, the fit is repeated in a reduced mass window of $\pm 700\,\mathrm{MeV}/c^2$ around the world average B meson mass. The result is found to be statistically consistent with the nominal fit. Combining these systematic effects, an overall $(^{+2.0}_{-1.8})\%$ relative uncertainty on the yield ratio is found.

The efficiency ratio can be factorised as

$$\frac{\epsilon_{B_s^0\to\phi\gamma}}{\epsilon_{B^0\to K^{*0}\gamma}} = r_{\mathrm{reco\&sel}} \times r_{\mathrm{PID}} \times r_{\mathrm{trigger}}, \tag{3}$$

where $r_{\mathrm{reco\&sel}}$, r_{PID} and r_{trigger} are the efficiency ratios due to the reconstruction and selection requirements, the particle identification (PID) requirements and the trigger requirements, respectively.

The correlated acceptance of the kaons due to the limited phase-space in the $\phi \to K^+K^-$ decay causes the ϕ vertex to have a worse spatial resolution than the K^{*0} vertex. This affects the $B_s^0 \to \phi\gamma$ selection efficiency through the IP χ^2 and vertex isolation cuts, while the common track cut $p_{\mathrm{T}} > 500\,\mathrm{MeV}/c$ is less efficient on the softer pion from the K^{*0} decay. These effects partially cancel and the reconstruction and selection efficiency ratio is found to be $r_{\mathrm{reco\&sel}} = 0.906 \pm 0.007\,(\mathrm{stat.}) \pm 0.017\,(\mathrm{syst.})$. The majority of the systematic uncertainties also cancel, since the kinematic selections are almost identical for both decays. The remaining systematic uncertainties include the hadron reconstruction efficiency, arising from differences in the

Table 2
Summary of the individual contributions to the relative systematic uncertainty on the ratio of branching fractions as defined in Eq. (2).

Uncertainty source	Systematic uncertainty
$r_{\text{reco\&sel}}$	2.0%
r_{PID}	1.3%
r_{trigger}	0.8%
$\mathcal{B}(\phi \to \text{K}^+\text{K}^-)/\mathcal{B}(\text{K}^{*0} \to \text{K}^+\pi^-)$	1.1%
Signal and background modelling	$^{+2.0}_{-1.8}$%
Total	3.4%

interaction of pions and kaons with the detector and uncertainties in the description of the detector material. The reliability of the simulation in describing the IP χ^2 of the tracks and the isolation of the B vertex is also included in the systematic uncertainty on the $r_{\text{reco\&sel}}$ ratio. The simulated samples are weighted for each signal and background contribution to reproduce the reconstructed mass distribution seen in data. No further systematic uncertainties are associated with the use of the simulation, since kinematic properties of the decays are observed to be well modelled. Uncertainties associated with the photon are negligible, because the reconstruction is identical in both decays.

The PID efficiency ratio is determined from data by means of a calibration procedure using pure samples of kaons and pions from $D^{*\pm} \to D^0(K^+\pi^-)\pi^\pm$ decays selected without PID information. This procedure yields $r_{\text{PID}} = 0.839 \pm 0.005\,(\text{stat.}) \pm 0.010\,(\text{syst.})$.

The trigger efficiency ratio $r_{\text{trigger}} = 1.080 \pm 0.009\,(\text{stat.})$ is obtained from the simulation. The systematic uncertainty due to any difference in the efficiency of the requirements made at the trigger level is included as part of the selection uncertainty.

Finally, the ratio of branching fractions is obtained using Eq. (2),

$$\frac{\mathcal{B}(B^0 \to K^{*0}\gamma)}{\mathcal{B}(B_s^0 \to \phi\gamma)} = 1.23 \pm 0.06\,(\text{stat.}) \pm 0.04\,(\text{syst.}) \pm 0.10\,(f_s/f_d),$$

where the first uncertainty is statistical, the second is the experimental systematic uncertainty and the third is due to the uncertainty on f_s/f_d. The contributions to the systematic uncertainty are summarised in Table 2.

6. Measurement of the *CP* asymmetry in $B^0 \to K^{*0}\gamma$ decays

The $B^0 \to K^{*0}\gamma$ and $\bar{B}^0 \to \bar{K}^{*0}\gamma$ invariant-mass distributions are fitted simultaneously to measure a raw asymmetry defined as

$$\mathcal{A}_{\text{RAW}} = \frac{N(K^-\pi^+\gamma) - N(K^+\pi^-\gamma)}{N(K^-\pi^+\gamma) + N(K^+\pi^-\gamma)}, \tag{4}$$

where $N(X)$ is the signal yield measured in the final state X. This asymmetry must be corrected for detection and production effects to measure the physical *CP* asymmetry. The detection asymmetry arises mainly from the kaon quark content giving a different interaction rate with the detector material depending on its charge. The B^0 and $\bar{B}^0$ mesons may also not be produced with the same rate in the region covered by the LHCb detector, inducing the B^0 meson production asymmetry. The physical *CP* asymmetry and these two corrections are related through

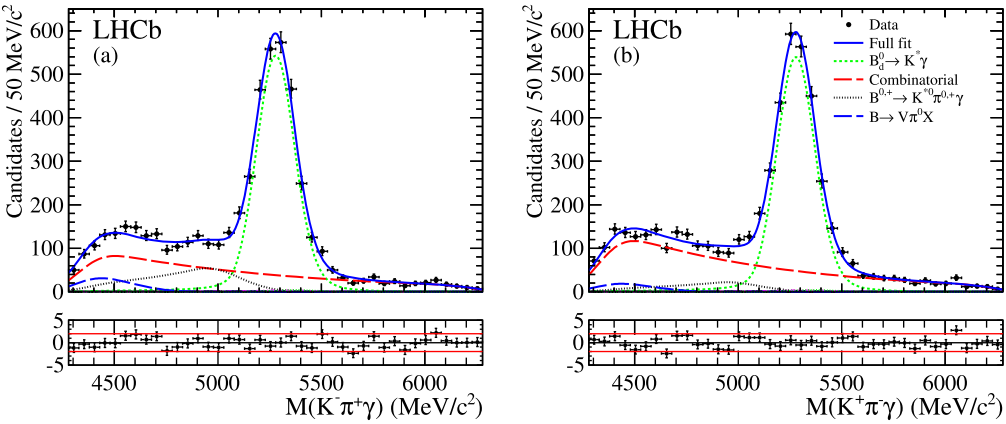

Fig. 3. Invariant-mass distributions of the (a) $\bar{B}^0 \to \bar{K}^{*0}\gamma$ and (b) $B^0 \to K^{*0}\gamma$ decay candidates. The black points represent the data and the fit result is represented as a solid blue line. The different background components are also shown. The Poisson χ^2 residuals [22] are shown below the fits with the $\pm 2\sigma$ confidence-level interval delimited by solid red lines. (For interpretation of the references to colours in this figure, the reader is referred to the web version of this article.)

$$\mathcal{A}_{CP}\big(B^0 \to K^{*0}\gamma\big) = \mathcal{A}_{\rm RAW}\big(B^0 \to K^{*0}\gamma\big) - \mathcal{A}_{\rm D}(K\pi) - \kappa\mathcal{A}_{\rm P}\big(B^0\big), \tag{5}$$

where $\mathcal{A}_{\rm D}(K\pi)$ and $\mathcal{A}_{\rm P}(B^0)$ represent the detection asymmetry of the kaon and pion pair and B^0 meson production asymmetry, respectively. The dilution factor κ arises from the oscillations of neutral B mesons.

To determine the raw asymmetry, the fit keeps the same signal mean and width, as well as the same mass-window threshold parameters for the B^0 and $\bar{B}^0$ signal. The yields of the combinatorial background and partially reconstructed decays are allowed to vary independently. The relative amplitudes of the exclusive peaking backgrounds, $\Lambda_b^0 \to \Lambda^*\gamma$, $B_s^0 \to K^{*0}\gamma$ and $B_{(s)}^0 \to K^+\pi^-\pi^0$, are fixed to the same values for both B flavours.

Fig. 3 shows the result of the simultaneous fit. The yields of the combinatorial background across the entire mass window are compatible within statistical uncertainty. The number of combinatorial background candidates is 2070 ± 414 and 1552 ± 422 in the full mass range for the $B^0 \to K^{*0}\gamma$ and $\bar{B}^0 \to \bar{K}^{*0}\gamma$ decays, respectively. The contribution from the charmless partially reconstructed decay $B^+ \to K^{*0}\pi^+\gamma$ to $B^0 \to K^{*0}\gamma$ and $\bar{B}^0 \to \bar{K}^{*0}\gamma$ is $(10 \pm 6)\%$ and $(24 \pm 7)\%$ of the signal yield, respectively. Furthermore, the charmed partially reconstructed decays $B \to K^{*0}\pi^0 X$ contribute with $(7 \pm 8)\%$ and $(9 \pm 8)\%$ of the signal yield to the $B^0 \to K^{*0}\gamma$ and $\bar{B}^0 \to \bar{K}^{*0}\gamma$ decays, respectively. The latter decays give contributions that are mainly located outside the signal invariant-mass region, as can be seen from Fig. 3.

The value of the raw asymmetry determined from the fit is $\mathcal{A}_{\rm RAW} = (0.3 \pm 1.7)\%$, where the uncertainty is statistical only.

The systematic uncertainty from the background modelling is determined as explained in Section 4. To address the systematic uncertainty from the possible CP asymmetry in the background, the yield of the $B^0 \to K^+\pi^-\pi^0$ decay is varied within its measured CP asymmetry $\mathcal{A}_{CP}(B^0 \to K^{*0}\pi^0) = (-15 \pm 12)\%$ [4]. For the other decays, a measurement of the CP asymmetry has not been made. The variation is therefore performed over the full $\pm 100\%$ range. The effect of these variations on $\mathcal{A}_{\rm RAW}$ gives rise to a Gaussian distribution centred at -0.2% with a standard deviation of 0.7%, thus a correction of $\Delta\mathcal{A}_{\rm bkg} = (-0.2 \pm 0.7)\%$ is applied. The

Table 3
CP asymmetry and total number of signal candidates measured for each magnet polarity.

	Magnet up	Magnet down
$\int \mathcal{L}\,dt$ (pb^{-1})	432 ± 15	588 ± 21
$\mathcal{A}^{\rm RAW}$ (%)	1.3 ± 2.6	-0.4 ± 2.2
Signal candidates	2189 ± 65	3103 ± 71

systematic uncertainty from the signal modelling is evaluated using a similar procedure and is found to be negligible. The possible double misidentification ($K^-\pi^+ \to \pi^-K^+$) in the final state would induce a dilution of the measured raw asymmetry. This is evaluated using simulated events and is also found to be negligible.

An instrumental bias can be caused by the vertical magnetic field, which deflects oppositely-charged particles into different regions of the detector. Any non-uniformity of the instrumental performance could introduce a bias in the asymmetry measurement. This potential bias is experimentally reduced by regularly changing the polarity of the magnetic field during data taking. As the integrated luminosity is slightly different for the "up" and "down" polarities, a residual bias could remain. This bias is studied by comparing the *CP* asymmetry measured separately in each of the samples collected with opposite magnet polarity, up or down. Table 3 summarises the *CP* asymmetry and the number of signal candidates for the two magnet polarities. The asymmetries with the two different polarities are determined to be compatible within the statistical uncertainties and the luminosity-weighted average, $\mathcal{A}_{\rm RAW} = (0.4 \pm 1.7)\%$, is in good agreement with the *CP* asymmetry measured in the full data sample.

The residual bias can be extracted from the polarity-split asymmetry as

$$\Delta\mathcal{A}_{\rm M} = \left(\frac{\mathcal{L}^{\rm up} - \mathcal{L}^{\rm down}}{\mathcal{L}^{\rm up} + \mathcal{L}^{\rm down}}\right)\left(\frac{\mathcal{A}^{\rm down}_{\rm RAW} - \mathcal{A}^{\rm up}_{\rm RAW}}{2}\right), \tag{6}$$

which is found to be consistent with zero $\Delta\mathcal{A}_{\rm M} = (+0.1 \pm 0.2)\%$. The raw asymmetry obtained from the fit is corrected by $\Delta\mathcal{A}_{\rm bkg}$ and $\Delta\mathcal{A}_{\rm M}$.

The detection asymmetry can be defined in terms of the detection efficiencies of the charge-conjugate final states by

$$\mathcal{A}_{\rm D}(K\pi) = \frac{\epsilon(K^-\pi^+) - \epsilon(K^+\pi^-)}{\epsilon(K^-\pi^+) + \epsilon(K^+\pi^-)}. \tag{7}$$

The related asymmetries have been studied at LHCb using control samples of charm decays [27]. It has been found that for $K\pi$ pairs in the kinematic range relevant for our analysis the detection asymmetry is $\mathcal{A}_{\rm D}(K\pi) = (-1.0 \pm 0.2)\%$.

The B production asymmetry is defined in terms of the different production rates

$$\mathcal{A}_{\rm P}\big(B^0\big) = \frac{R(\bar{B}^0) - R(B^0)}{R(\bar{B}^0) + R(B^0)} \tag{8}$$

and has been measured at LHCb to be $\mathcal{A}_{\rm P}(B^0) = (1.0 \pm 1.3)\%$ using large samples of $B^0 \to J/\psi K^{*0}$ decays [27]. The contribution of the production asymmetry to the measured *CP* asymmetry is diluted by a factor κ, defined as

$$\kappa = \frac{\int_0^\infty \cos(\Delta m_d t) e^{-\Gamma_d t}\epsilon(t)\,dt}{\int_0^\infty \cosh(\frac{\Delta\Gamma_d t}{2}) e^{-\Gamma_d t}\epsilon(t)\,dt}, \tag{9}$$

Table 4
Corrections to the raw asymmetry and corresponding systematic uncertainties.

Correction to $A_{\rm RAW}$		Value [%]
Background model	$\Delta\mathcal{A}_{\rm bkg}$	-0.2 ± 0.7
Magnet polarity	$\Delta\mathcal{A}_{\rm M}$	$+0.1 \pm 0.2$
Detection	$-\mathcal{A}_{\rm D}(K\pi)$	$+1.0 \pm 0.2$
B^0 production	$-\kappa\mathcal{A}_{\rm P}(B^0)$	-0.4 ± 0.5
Total		$+0.5 \pm 0.9$

where Δm_d and $\Delta\Gamma_d$ are the mass difference and the decay width difference between the mass eigenstates of the B^0–$\bar{B}^0$ system, Γ_d is the average of their decay widths and $\epsilon(t)$ is the decay-time acceptance function of the signal selection. The latter has been determined from data using the decay-time distribution of background-subtracted signal candidates, the known B^0 lifetime and assuming $\Delta\Gamma_d = 0$. The dilution factor is found to be $\kappa = 0.41 \pm 0.04$, where the uncertainty comes from knowledge of the acceptance function parameters as well as Γ_d and Δm_d.

Adding the above corrections, which are summarised in Table 4, to the raw asymmetry, the direct *CP* asymmetry in $B^0 \to K^{*0}\gamma$ decays is measured to be

$$\mathcal{A}_{CP}\big(B^0 \to K^{*0}\gamma\big) = \big(0.8 \pm 1.7\ (\text{stat.}) \pm 0.9\ (\text{syst.})\big)\%.$$

7. Results and conclusions

Using an integrated luminosity of 1.0 fb^{-1} of pp collision data collected by the LHCb experiment at a centre-of-mass energy of $\sqrt{s} = 7$ TeV, the ratio of branching fractions between $B^0 \to K^{*0}\gamma$ and $B_s^0 \to \phi\gamma$ has been measured to be

$$\frac{\mathcal{B}(B^0 \to K^{*0}\gamma)}{\mathcal{B}(B_s^0 \to \phi\gamma)} = 1.23 \pm 0.06\ (\text{stat.}) \pm 0.04\ (\text{syst.}) \pm 0.10\ (f_s/f_d),$$

which is the most precise measurement to date and is in good agreement with the SM prediction of 1.0 ± 0.2 [6].

Using the world average value $\mathcal{B}(B^0 \to K^{*0}\gamma) = (4.33 \pm 0.15) \times 10^{-5}$ [4], the $B_s^0 \to \phi\gamma$ branching fraction is determined to be

$$\mathcal{B}\big(B_s^0 \to \phi\gamma\big) = (3.5 \pm 0.4) \times 10^{-5},$$

in agreement with the previous measurement [3]. This is the most precise measurement to date and is consistent with, but supersedes, a previous LHCb result using an integrated luminosity of 0.37 fb^{-1} [11].

The direct *CP* asymmetry in $B^0 \to K^{*0}\gamma$ decays has also been measured with the same data sample and found to be

$$\mathcal{A}_{CP}\big(B^0 \to K^{*0}\gamma\big) = \big(0.8 \pm 1.7\ (\text{stat.}) \pm 0.9\ (\text{syst.})\big)\%,$$

in agreement with the SM expectation of $(-0.61 \pm 0.43)\%$ [8]. This is consistent with previous measurements [5], and is the most precise result of the direct *CP* asymmetry in $B^0 \to K^{*0}\gamma$ decays to date.

Acknowledgements

We express our gratitude to our colleagues in the CERN accelerator departments for the excellent performance of the LHC. We thank the technical and administrative staff at CERN and at the LHCb institutes, and acknowledge support from the National Agencies: CAPES, CNPq, FAPERJ and FINEP (Brazil); CERN; NSFC (China); CNRS/IN2P3 (France); BMBF, DFG, HGF and MPG (Germany); SFI (Ireland); INFN (Italy); FOM and NWO (The Netherlands); SCSR (Poland); ANCS (Romania); MinES of Russia and Rosatom (Russia); MICINN, XuntaGal and GENCAT (Spain); SNSF and SER (Switzerland); NAS Ukraine (Ukraine); STFC (United Kingdom); NSF (USA). We also acknowledge the support received from the ERC under FP7 and the Region Auvergne.

References

[1] S. Descotes-Genon, D. Ghosh, J. Matias, M. Ramon, Exploring new physics in the C_7–C_7' plane, JHEP 1106 (2011) 099, arXiv:1104.3342.

[2] CLEO Collaboration, R. Ammar, et al., Evidence for penguin-diagram decays: First observation of $B \to K^*(892)\gamma$, Phys. Rev. Lett. 71 (1993) 674.

[3] Belle Collaboration, J. Wicht, et al., Observation of $B_s^0 \to \phi\gamma$ and search for $B_s^0 \to \gamma\gamma$ decays at Belle, Phys. Rev. Lett. 100 (2008) 121801, arXiv:0712.2659.

[4] Heavy Flavor Averaging Group, Y. Amhis, et al., Averages of b-hadron, c-hadron, and tau-lepton properties as of early 2012, arXiv:1207.1158.

[5] BaBar Collaboration, B. Aubert, et al., Measurement of branching fractions and CP and isospin asymmetries in $B \to K^*(892)\gamma$ decays, Phys. Rev. Lett. 103 (2009) 211802, arXiv:0906.2177;
Belle Collaboration, M. Nakao, et al., Measurement of the $B \to K^*\gamma$ branching fractions and asymmetries, Phys. Rev. D 69 (2004) 112001, arXiv:hep-ex/0402042;
CLEO Collaboration, T. Coan, et al., Study of exclusive radiative B meson decays, Phys. Rev. Lett. 84 (2000) 5283, arXiv:hep-ex/9912057.

[6] A. Ali, B.D. Pecjak, C. Greub, Towards $B \to V\gamma$ decays at NNLO in SCET, Eur. Phys. J. C 55 (2008) 577, arXiv:0709.4422.

[7] K. de Bruyn, et al., Branching ratio measurements of B_s decays, Phys. Rev. D 86 (2012) 014027, arXiv:1204.1735.

[8] M. Matsumori, A.I. Sanda, Y.Y. Keum, *CP* asymmetry, branching ratios and isospin breaking effects of $B^0 \to K^{*0}\gamma$ with perturbative QCD approach, Phys. Rev. D 72 (2005) 014013, arXiv:hep-ph/0406055.

[9] Particle Data Group, J. Beringer, et al., Review of particle physics, Phys. Rev. D 86 (2012) 010001.

[10] C. Dariescu, M.-A. Dariescu, $B^0 \to K^{*0}\gamma$ decay within MSSM, arXiv:0710.3819;
M. Aoki, G.-C. Cho, N. Oshimo, Decay rate asymmetry in $B \to X_s\gamma$ as a signature of supersymmetry, Phys. Rev. D 60 (1999) 035004, arXiv:hep-ph/9811251;
M. Aoki, G.-C. Cho, N. Oshimo, *CP* asymmetry for radiative B meson decay in the supersymmetric standard model, Nucl. Phys. B 554 (1999) 50, arXiv:hep-ph/9903385;
A.L. Kagan, M. Neubert, Direct *CP* violation in $B \to X_s\gamma$ decays as a signature of new physics, Phys. Rev. D 58 (1998) 094012, arXiv:hep-ph/9803368.

[11] LHCb Collaboration, R. Aaij, et al., Measurement of the ratio of branching fractions $\mathcal{B}(B^0 \to K^{*0}\gamma)/\mathcal{B}(B_s^0 \to \phi\gamma)$, Phys. Rev. D 85 (2012) 112013, arXiv:1202.6267.

[12] LHCb Collaboration, A.A. Alves Jr., et al., The LHCb detector at the LHC, JINST 3 (2008) S08005.

[13] T. Sjöstrand, S. Mrenna, P. Skands, PYTHIA 6.4 physics and manual, JHEP 0605 (2006) 026, arXiv:hep-ph/0603175.

[14] I. Belyaev, et al., Handling of the generation of primary events in GAUSS, the LHCb simulation framework, IEEE Nucl. Sci. Symp. Conf. Rec. (NSS/MIC) (2010) 1155.
[15] D.J. Lange, The EvtGen particle decay simulation package, Nucl. Instrum. Meth. A 462 (2001) 152.
[16] P. Golonka, Z. Was, PHOTOS Monte Carlo: A precision tool for QED corrections in Z and W decays, Eur. Phys. J. C 45 (2006) 97, arXiv:hep-ph/0506026.
[17] GEANT4 Collaboration, J. Allison, et al., Geant4 developments and applications, IEEE Trans. Nucl. Sci. 53 (2006) 270;
GEANT4 Collaboration, S. Agostinelli, et al., GEANT4: A simulation toolkit, Nucl. Instrum. Meth. A 506 (2003) 250.
[18] M. Clemencic, et al., The LHCb simulation application, Gauss: Design, evolution and experience, J. Phys. Conf. Ser. 331 (2011) 032023.
[19] O. Deschamps, et al., Photon and neutral pion reconstruction, LHCb-2003-091.
[20] LHCb Collaboration, R. Aaij, et al., Measurement of b-hadron masses, Phys. Lett. B 708 (2012) 241, arXiv:1112.4896.
[21] HERA-B Collaboration, I. Abt, et al., K^{*0} and ϕ meson production in proton–nucleus interactions at $\sqrt{s} = 41.6$ GeV, Eur. Phys. J. C 50 (2007) 315, arXiv:hep-ex/0606049.
[22] S. Baker, R.D. Cousins, Clarification of the use of chi-square and likelihood functions in fits to histograms, Nucl. Instrum. Meth. A 221 (1984) 437.
[23] T. Skwarnicki, A study of the radiative cascade transitions between the Upsilon-prime and Upsilon resonances, PhD thesis, Institute of Nuclear Physics, Krakow, 1986, DESY-F31-86-02.
[24] ARGUS Collaboration, H. Albrecht, et al., Search for hadronic $b \to u$ decays, Phys. Lett. B 241 (1990) 278.
[25] P. Ball, G.W. Jones, R. Zwicky, $B \to V\gamma$ beyond QCD factorization, Phys. Rev. D 75 (2007) 054004, arXiv:hep-ph/0612081.
[26] LHCb Collaboration, R. Aaij, et al., Measurement of b hadron production fractions in 7 TeV pp collisions, Phys. Rev. D 85 (2012) 032008, arXiv:1111.2357.
[27] LHCb Collaboration, Measurement of direct CP violation in charmless charged two-body B decays at LHCb using 2010 data, LHCb-CONF-2011-042.

LHCb Collaboration

R. Aaij [38], C. Abellan Beteta [33,n], A. Adametz [11], B. Adeva [34], M. Adinolfi [43], C. Adrover [6], A. Affolder [49], Z. Ajaltouni [5], J. Albrecht [35], F. Alessio [35], M. Alexander [48], S. Ali [38], G. Alkhazov [27], P. Alvarez Cartelle [34], A.A. Alves Jr. [22], S. Amato [2], Y. Amhis [36], L. Anderlini [17,f], J. Anderson [37], R.B. Appleby [51], O. Aquines Gutierrez [10], F. Archilli [18,35], A. Artamonov [32], M. Artuso [53], E. Aslanides [6], G. Auriemma [22,m], S. Bachmann [11], J.J. Back [45], C. Baesso [54], V. Balagura [28], W. Baldini [16], R.J. Barlow [51], C. Barschel [35], S. Barsuk [7], W. Barter [44], A. Bates [48], C. Bauer [10], Th. Bauer [38], A. Bay [36], J. Beddow [48], I. Bediaga [1], S. Belogurov [28], K. Belous [32], I. Belyaev [28], E. Ben-Haim [8], M. Benayoun [8], G. Bencivenni [18], S. Benson [47], J. Benton [43], A. Berezhnoy [29], R. Bernet [37], M.-O. Bettler [44], M. van Beuzekom [38], A. Bien [11], S. Bifani [12], T. Bird [51], A. Bizzeti [17,h], P.M. Bjørnstad [51], T. Blake [35], F. Blanc [36], C. Blanks [50], J. Blouw [11], S. Blusk [53], A. Bobrov [31], V. Bocci [22], A. Bondar [31], N. Bondar [27], W. Bonivento [15], S. Borghi [48,51], A. Borgia [53], T.J.V. Bowcock [49], C. Bozzi [16], T. Brambach [9], J. van den Brand [39], J. Bressieux [36], D. Brett [51], M. Britsch [10], T. Britton [53], N.H. Brook [43], H. Brown [49], A. Büchler-Germann [37], I. Burducea [26],

A. Bursche [37], J. Buytaert [35], S. Cadeddu [15], O. Callot [7], M. Calvi [20,j], M. Calvo Gomez [33,n], A. Camboni [33], P. Campana [18,35], A. Carbone [14,c], G. Carboni [21,k], R. Cardinale [19,35,i], A. Cardini [15], L. Carson [50], K. Carvalho Akiba [2], G. Casse [49], M. Cattaneo [35], Ch. Cauet [9], M. Charles [52], Ph. Charpentier [35], P. Chen [3,36], N. Chiapolini [37], M. Chrzaszcz [23], K. Ciba [35], X. Cid Vidal [34], G. Ciezarek [50], P.E.L. Clarke [47], M. Clemencic [35], H.V. Cliff [44], J. Closier [35], C. Coca [26], V. Coco [38], J. Cogan [6], E. Cogneras [5], P. Collins [35], A. Comerma-Montells [33], A. Contu [52], A. Cook [43], M. Coombes [43], G. Corti [35], B. Couturier [35], G.A. Cowan [36], D. Craik [45], S. Cunliffe [50], R. Currie [47], C. D'Ambrosio [35], P. David [8], P.N.Y. David [38], I. De Bonis [4], K. De Bruyn [38], S. De Capua [21,k], M. De Cian [37], J.M. De Miranda [1], L. De Paula [2], P. De Simone [18], D. Decamp [4], M. Deckenhoff [9], H. Degaudenzi [36,35], L. Del Buono [8], C. Deplano [15], D. Derkach [14,35], O. Deschamps [5], F. Dettori [39], J. Dickens [44], H. Dijkstra [35], P. Diniz Batista [1], F. Domingo Bonal [33,n], S. Donleavy [49], F. Dordei [11], A. Dosil Suárez [34], D. Dossett [45], A. Dovbnya [40], F. Dupertuis [36], R. Dzhelyadin [32], A. Dziurda [23], A. Dzyuba [27], S. Easo [46], U. Egede [50], V. Egorychev [28], S. Eidelman [31], D. van Eijk [38], F. Eisele [11], S. Eisenhardt [47], R. Ekelhof [9], L. Eklund [48], I. El Rifai [5], Ch. Elsasser [37], D. Elsby [42], D. Esperante Pereira [34], A. Falabella [14,e], C. Färber [11], G. Fardell [47], C. Farinelli [38], S. Farry [12], V. Fave [36], V. Fernandez Albor [34], F. Ferreira Rodrigues [1], M. Ferro-Luzzi [35], S. Filippov [30], C. Fitzpatrick [47], M. Fontana [10], F. Fontanelli [19,i], R. Forty [35], O. Francisco [2], M. Frank [35], C. Frei [35], M. Frosini [17,f], S. Furcas [20], A. Gallas Torreira [34], D. Galli [14,c], M. Gandelman [2], P. Gandini [52], Y. Gao [3], J.-C. Garnier [35], J. Garofoli [53], J. Garra Tico [44], L. Garrido [33], D. Gascon [33], C. Gaspar [35], R. Gauld [52], E. Gersabeck [11], M. Gersabeck [35], T. Gershon [45,35], Ph. Ghez [4], V. Gibson [44], V.V. Gligorov [35], C. Göbel [54], D. Golubkov [28], A. Golutvin [50,28,35], A. Gomes [2], H. Gordon [52], M. Grabalosa Gándara [33], R. Graciani Diaz [33], L.A. Granado Cardoso [35], E. Graugés [33], G. Graziani [17], A. Grecu [26], E. Greening [52], S. Gregson [44], O. Grünberg [55], B. Gui [53], E. Gushchin [30], Yu. Guz [32], T. Gys [35], C. Hadjivasiliou [53], G. Haefeli [36], C. Haen [35], S.C. Haines [44], S. Hall [50], T. Hampson [43], S. Hansmann-Menzemer [11], N. Harnew [52], S.T. Harnew [43], J. Harrison [51], P.F. Harrison [45], T. Hartmann [55], J. He [7], V. Heijne [38], K. Hennessy [49], P. Henrard [5], J.A. Hernando Morata [34], E. van Herwijnen [35], E. Hicks [49],

D. Hill [52], M. Hoballah [5], P. Hopchev [4], W. Hulsbergen [38], P. Hunt [52], T. Huse [49], N. Hussain [52], R.S. Huston [12], D. Hutchcroft [49], D. Hynds [48], V. Iakovenko [41], P. Ilten [12], J. Imong [43], R. Jacobsson [35], A. Jaeger [11], M. Jahjah Hussein [5], E. Jans [38], F. Jansen [38], P. Jaton [36], B. Jean-Marie [7], F. Jing [3], M. John [52], D. Johnson [52], C.R. Jones [44], B. Jost [35], M. Kaballo [9], S. Kandybei [40], M. Karacson [35], T.M. Karbach [9], J. Keaveney [12], I.R. Kenyon [42], U. Kerzel [35], T. Ketel [39], A. Keune [36], B. Khanji [20], Y.M. Kim [47], M. Knecht [36], O. Kochebina [7], I. Komarov [29], R.F. Koopman [39], P. Koppenburg [38], M. Korolev [29], A. Kozlinskiy [38], L. Kravchuk [30], K. Kreplin [11], M. Kreps [45], G. Krocker [11], P. Krokovny [31], F. Kruse [9], M. Kucharczyk [20,23,35,j], V. Kudryavtsev [31], T. Kvaratskheliya [28,35], V.N. La Thi [36], D. Lacarrere [35], G. Lafferty [51], A. Lai [15], D. Lambert [47], R.W. Lambert [39], E. Lanciotti [35], G. Lanfranchi [18,35], C. Langenbruch [35], T. Latham [45], C. Lazzeroni [42], R. Le Gac [6], J. van Leerdam [38], J.-P. Lees [4], R. Lefèvre [5], A. Leflat [29,35], J. Lefrançois [7], O. Leroy [6], T. Lesiak [23], L. Li [3], Y. Li [3], L. Li Gioi [5], M. Lieng [9], M. Liles [49], R. Lindner [35], C. Linn [11], B. Liu [3], G. Liu [35], J. von Loeben [20], J.H. Lopes [2], E. Lopez Asamar [33], N. Lopez-March [36], H. Lu [3], J. Luisier [36], A. Mac Raighne [48], F. Machefert [7], I.V. Machikhiliyan [4,28], F. Maciuc [10], O. Maev [27,35], J. Magnin [1], S. Malde [52], R.M.D. Mamunur [35], G. Manca [15,d], G. Mancinelli [6], N. Mangiafave [44], U. Marconi [14], R. Märki [36], J. Marks [11], G. Martellotti [22], A. Martens [8], L. Martin [52], A. Martín Sánchez [7], M. Martinelli [38], D. Martinez Santos [35], A. Massafferri [1], Z. Mathe [12], C. Matteuzzi [20], M. Matveev [27], E. Maurice [6], A. Mazurov [16,30,35], J. McCarthy [42], G. McGregor [51], R. McNulty [12], M. Meissner [11], M. Merk [38], J. Merkel [9], D.A. Milanes [13], M.-N. Minard [4], J. Molina Rodriguez [54], S. Monteil [5], D. Moran [51], P. Morawski [23], R. Mountain [53], I. Mous [38], F. Muheim [47], K. Müller [37], R. Muresan [26], B. Muryn [24], B. Muster [36], J. Mylroie-Smith [49], P. Naik [43], T. Nakada [36], R. Nandakumar [46], I. Nasteva [1], M. Needham [47], N. Neufeld [35], A.D. Nguyen [36], C. Nguyen-Mau [36,o], M. Nicol [7], V. Niess [5], N. Nikitin [29], T. Nikodem [11], A. Nomerotski [52,35], A. Novoselov [32], A. Oblakowska-Mucha [24], V. Obraztsov [32], S. Oggero [38], S. Ogilvy [48], O. Okhrimenko [41], R. Oldeman [15,35,d], M. Orlandea [26], J.M. Otalora Goicochea [2], P. Owen [50], B.K. Pal [53], A. Palano [13,b], M. Palutan [18], J. Panman [35], A. Papanestis [46], M. Pappagallo [48], C. Parkes [51], C.J. Parkinson [50], G. Passaleva [17],

G.D. Patel [49], M. Patel [50], G.N. Patrick [46], C. Patrignani [19,i], C. Pavel-Nicorescu [26], A. Pazos Alvarez [34], A. Pellegrino [38], G. Penso [22,l], M. Pepe Altarelli [35], S. Perazzini [14,c], D.L. Perego [20,j], E. Perez Trigo [34], A. Pérez-Calero Yzquierdo [33], P. Perret [5], M. Perrin-Terrin [6], G. Pessina [20], A. Petrolini [19,i], A. Phan [53], E. Picatoste Olloqui [33], B. Pie Valls [33], B. Pietrzyk [4], T. Pilař [45], D. Pinci [22], S. Playfer [47], M. Plo Casasus [34], F. Polci [8], G. Polok [23], A. Poluektov [45,31], E. Polycarpo [2], D. Popov [10], B. Popovici [26], C. Potterat [33], A. Powell [52], J. Prisciandaro [36], V. Pugatch [41], A. Puig Navarro [33], W. Qian [3], J.H. Rademacker [43], B. Rakotomiaramanana [36], M.S. Rangel [2], I. Raniuk [40], N. Rauschmayr [35], G. Raven [39], S. Redford [52], M.M. Reid [45], A.C. dos Reis [1], S. Ricciardi [46], A. Richards [50], K. Rinnert [49], D.A. Roa Romero [5], P. Robbe [7], E. Rodrigues [48,51], P. Rodriguez Perez [34], G.J. Rogers [44], S. Roiser [35], V. Romanovsky [32], A. Romero Vidal [34], M. Rosello [33,n], J. Rouvinet [36], T. Ruf [35], H. Ruiz [33], G. Sabatino [21,k], J.J. Saborido Silva [34], N. Sagidova [27], P. Sail [48], B. Saitta [15,d], C. Salzmann [37], B. Sanmartin Sedes [34], M. Sannino [19,i], R. Santacesaria [22], C. Santamarina Rios [34], R. Santinelli [35], E. Santovetti [21,k], M. Sapunov [6], A. Sarti [18,l], C. Satriano [22,m], A. Satta [21], M. Savrie [16,e], D. Savrina [28], P. Schaack [50], M. Schiller [39], H. Schindler [35], S. Schleich [9], M. Schlupp [9], M. Schmelling [10], B. Schmidt [35], O. Schneider [36], A. Schopper [35], M.-H. Schune [7], R. Schwemmer [35], B. Sciascia [18], A. Sciubba [18,l], M. Seco [34], A. Semennikov [28], K. Senderowska [24], I. Sepp [50], N. Serra [37], J. Serrano [6], P. Seyfert [11], M. Shapkin [32], I. Shapoval [40,35], P. Shatalov [28], Y. Shcheglov [27], T. Shears [49], L. Shekhtman [31], O. Shevchenko [40], V. Shevchenko [28], A. Shires [50], R. Silva Coutinho [45], T. Skwarnicki [53], N.A. Smith [49], E. Smith [52,46], M. Smith [51], K. Sobczak [5], F.J.P. Soler [48], A. Solomin [43], F. Soomro [18,35], D. Souza [43], B. Souza De Paula [2], B. Spaan [9], A. Sparkes [47], P. Spradlin [48], F. Stagni [35], S. Stahl [11], O. Steinkamp [37], S. Stoica [26], S. Stone [53], B. Storaci [38], M. Straticiuc [26], U. Straumann [37], V.K. Subbiah [35], S. Swientek [9], M. Szczekowski [25], P. Szczypka [36,35], T. Szumlak [24], S. T'Jampens [4], M. Teklishyn [7], E. Teodorescu [26], F. Teubert [35], C. Thomas [52], E. Thomas [35], J. van Tilburg [11], V. Tisserand [4], M. Tobin [37], S. Tolk [39], S. Topp-Joergensen [52], N. Torr [52], E. Tournefier [4,50], S. Tourneur [36], M.T. Tran [36], A. Tsaregorodtsev [6], N. Tuning [38], M. Ubeda Garcia [35], A. Ukleja [25], U. Uwer [11], V. Vagnoni [14], G. Valenti [14], R. Vazquez Gomez [33,*], P. Vazquez Regueiro [34], S. Vecchi [16],

J.J. Velthuis [43], M. Veltri [17,g], G. Veneziano [36], M. Vesterinen [35], B. Viaud [7], I. Videau [7], D. Vieira [2], X. Vilasis-Cardona [33,n], J. Visniakov [34], A. Vollhardt [37], D. Volyanskyy [10], D. Voong [43], A. Vorobyev [27], V. Vorobyev [31], C. Voß [55], H. Voss [10], R. Waldi [55], R. Wallace [12], S. Wandernoth [11], J. Wang [53], D.R. Ward [44], N.K. Watson [42], A.D. Webber [51], D. Websdale [50], M. Whitehead [45], J. Wicht [35], D. Wiedner [11], L. Wiggers [38], G. Wilkinson [52], M.P. Williams [45,46], M. Williams [50], F.F. Wilson [46], J. Wishahi [9], M. Witek [23], W. Witzeling [35], S.A. Wotton [44], S. Wright [44], S. Wu [3], K. Wyllie [35], Y. Xie [47], F. Xing [52], Z. Xing [53], Z. Yang [3], R. Young [47], X. Yuan [3], O. Yushchenko [32], M. Zangoli [14], M. Zavertyaev [10,a], F. Zhang [3], L. Zhang [53], W.C. Zhang [12], Y. Zhang [3], A. Zhelezov [11], L. Zhong [3], A. Zvyagin [35]

[1] *Centro Brasileiro de Pesquisas Físicas (CBPF), Rio de Janeiro, Brazil*
[2] *Universidade Federal do Rio de Janeiro (UFRJ), Rio de Janeiro, Brazil*
[3] *Center for High Energy Physics, Tsinghua University, Beijing, China*
[4] *LAPP, Université de Savoie, CNRS/IN2P3, Annecy-Le-Vieux, France*
[5] *Clermont Université, Université Blaise Pascal, CNRS/IN2P3, LPC, Clermont-Ferrand, France*
[6] *CPPM, Aix-Marseille Université, CNRS/IN2P3, Marseille, France*
[7] *LAL, Université Paris-Sud, CNRS/IN2P3, Orsay, France*
[8] *LPNHE, Université Pierre et Marie Curie, Université Paris Diderot, CNRS/IN2P3, Paris, France*
[9] *Fakultät Physik, Technische Universität Dortmund, Dortmund, Germany*
[10] *Max-Planck-Institut für Kernphysik (MPIK), Heidelberg, Germany*
[11] *Physikalisches Institut, Ruprecht-Karls-Universität Heidelberg, Heidelberg, Germany*
[12] *School of Physics, University College Dublin, Dublin, Ireland*
[13] *Sezione INFN di Bari, Bari, Italy*
[14] *Sezione INFN di Bologna, Bologna, Italy*
[15] *Sezione INFN di Cagliari, Cagliari, Italy*
[16] *Sezione INFN di Ferrara, Ferrara, Italy*
[17] *Sezione INFN di Firenze, Firenze, Italy*
[18] *Laboratori Nazionali dell'INFN di Frascati, Frascati, Italy*
[19] *Sezione INFN di Genova, Genova, Italy*
[20] *Sezione INFN di Milano Bicocca, Milano, Italy*
[21] *Sezione INFN di Roma Tor Vergata, Roma, Italy*
[22] *Sezione INFN di Roma La Sapienza, Roma, Italy*
[23] *Henryk Niewodniczanski Institute of Nuclear Physics Polish Academy of Sciences, Kraków, Poland*
[24] *AGH University of Science and Technology, Kraków, Poland*
[25] *Soltan Institute for Nuclear Studies, Warsaw, Poland*
[26] *Horia Hulubei National Institute of Physics and Nuclear Engineering, Bucharest-Magurele, Romania*
[27] *Petersburg Nuclear Physics Institute (PNPI), Gatchina, Russia*
[28] *Institute of Theoretical and Experimental Physics (ITEP), Moscow, Russia*
[29] *Institute of Nuclear Physics, Moscow State University (SINP MSU), Moscow, Russia*
[30] *Institute for Nuclear Research of the Russian Academy of Sciences (INR RAN), Moscow, Russia*
[31] *Budker Institute of Nuclear Physics (SB RAS) and Novosibirsk State University, Novosibirsk, Russia*
[32] *Institute for High Energy Physics (IHEP), Protvino, Russia*
[33] *Universitat de Barcelona, Barcelona, Spain*
[34] *Universidad de Santiago de Compostela, Santiago de Compostela, Spain*
[35] *European Organization for Nuclear Research (CERN), Geneva, Switzerland*
[36] *Ecole Polytechnique Fédérale de Lausanne (EPFL), Lausanne, Switzerland*
[37] *Physik-Institut, Universität Zürich, Zürich, Switzerland*

[38] *Nikhef National Institute for Subatomic Physics, Amsterdam, The Netherlands*
[39] *Nikhef National Institute for Subatomic Physics and VU University Amsterdam, Amsterdam, The Netherlands*
[40] *NSC Kharkiv Institute of Physics and Technology (NSC KIPT), Kharkiv, Ukraine*
[41] *Institute for Nuclear Research of the National Academy of Sciences (KINR), Kyiv, Ukraine*
[42] *University of Birmingham, Birmingham, United Kingdom*
[43] *H.H. Wills Physics Laboratory, University of Bristol, Bristol, United Kingdom*
[44] *Cavendish Laboratory, University of Cambridge, Cambridge, United Kingdom*
[45] *Department of Physics, University of Warwick, Coventry, United Kingdom*
[46] *STFC Rutherford Appleton Laboratory, Didcot, United Kingdom*
[47] *School of Physics and Astronomy, University of Edinburgh, Edinburgh, United Kingdom*
[48] *School of Physics and Astronomy, University of Glasgow, Glasgow, United Kingdom*
[49] *Oliver Lodge Laboratory, University of Liverpool, Liverpool, United Kingdom*
[50] *Imperial College London, London, United Kingdom*
[51] *School of Physics and Astronomy, University of Manchester, Manchester, United Kingdom*
[52] *Department of Physics, University of Oxford, Oxford, United Kingdom*
[53] *Syracuse University, Syracuse, NY, United States*
[54] *Pontifícia Universidade Católica do Rio de Janeiro (PUC-Rio), Rio de Janeiro, Brazil* [p]
[55] *Institut für Physik, Universität Rostock, Rostock, Germany* [q]

[*] Corresponding author.
E-mail address: rvazquez@cern.ch (R. Vazquez Gomez).
[a] P.N. Lebedev Physical Institute, Russian Academy of Science (LPI RAS), Moscow, Russia.
[b] Università di Bari, Bari, Italy.
[c] Università di Bologna, Bologna, Italy.
[d] Università di Cagliari, Cagliari, Italy.
[e] Università di Ferrara, Ferrara, Italy.
[f] Università di Firenze, Firenze, Italy.
[g] Università di Urbino, Urbino, Italy.
[h] Università di Modena e Reggio Emilia, Modena, Italy.
[i] Università di Genova, Genova, Italy.
[j] Università di Milano Bicocca, Milano, Italy.
[k] Università di Roma Tor Vergata, Roma, Italy.
[l] Università di Roma La Sapienza, Roma, Italy.
[m] Università della Basilicata, Potenza, Italy.
[n] LIFAELS, La Salle, Universitat Ramon Llull, Barcelona, Spain.
[o] Hanoi University of Science, Hanoi, Viet Nam.
[p] Associated to Universidade Federal do Rio de Janeiro (UFRJ), Rio de Janeiro, Brazil.
[q] Associated to Physikalisches Institut, Ruprecht-Karls-Universität Heidelberg, Heidelberg, Germany.